

Experimental analysis of the breakage of a liquid bridge under microgravity conditions

I. Martínez , J.M. Perales

^a Instituto de Microgravedad "Ignacio Da Riva", Universidad Politécnica de Madrid, Madrid, Spain

^b E.T.S.I.Aeronáuticos, Universidad Politécnica de Madrid, Madrid, Spain

Abstract

The experimental results obtained in experiment "STACO" made on board the Spacelab D-2 are re-visited, with image-analysis tools not then available. The configuration consisted of a liquid bridge between two solid supporting discs. An expected breakage occurred during the experiment. The recorded images are analysed and the measured behaviour compared with the results of a three dimensional model of the liquid dynamics, obtaining a much better fit than with linear models.

Keywords: Capillarity; Experimental; Microgravity; Liquid bridge; Liquid column

1. Introduction

Fluid science experiments in space are still scarce and costly, what justifies trying to get the most of what is available, as done here with experiment SL-D2-WL-AFPM-STACO-run2: the second run of an experiment on the STABILITY of liquid COLUMNS, performed with ESA's Advanced Fluid Physics Module, located within the German WerkstoffLabor, in Spacelab D-2 mission, aboard Columbia STS-55, with Ulrich Walter as space operator, Gerhard Thiele as crew coordinator on ground, and I. Martínez and J.M. Perales at the ground control centre in Oberpfaffenhofen (from a 1985 proposal by I. Martínez, J. Meseguer and J.M. Perales).

This space experiment belongs to a series on the behaviour of long liquid columns under microgravity, when subjected to some mechanical disturbances: stretching, rotation, vibration, etc. After preliminary trials aboard Spacelab in 1983 and Spacelab D-1 in 1985, we learnt that

measuring the response to the uncontrolled mechanical noise (g-jitter) due to the new operational environment was a prerequisite. The aim of this second run of Staco experiment was to perform a controlled breaking of the liquid column by disc separation (the first run was devoted to the oscillatory response, and the third run to the stability with unequal discs). Experiments on liquid bridge breaking date back to Plateau's research with neutrally buoyant immiscible liquids in mid 19th century, but main interest arose in the second half of 20th century with its possible application to the containerless technique of crystal growth by the floating zone technique in materials science. Different analytical and numerical simulations have been developed to study this breaking process, as Meseguer (1983), Rivas and Meseguer (1984), Zhang et al. (1996), and others.

A liquid bridge is any liquid mass joining two separated solid surfaces within a free surface boundary. Gravity on ground prevents liquid bridges larger than a few millimetres (the capillary length $l_c = \sqrt{\sigma/(\rho g)}$, with σ surface tension, ρ density, and g gravity acceleration), but one may have liquid bridges of any size in weightlessness; we have built several liquid columns 85 mm long and 30 mm in

diameter, lasting typically one hour in Spacelab (Martínez et al., 2005) and 6 min on Texas sounding rockets (Martínez et al., 2004).

The experiment sequence we consider here (Staco run 2) corresponds to an already established liquid column subjected for a while (140 s) to background noise (we learnt from previous trials that, before applying any desired disturbance, sensing environmental disturbances is a must), and afterwards subjected to disc separation at constant volume until breaking the liquid bridge. This was already analysed when the flight results were reported in Martínez et al. (1995), but at that time the tools available for image analysis were rather crude (we could just digitize full individual frames or series of video lines). Now we have performed a full video digitization (Martínez, 2010), and automated full-image analysis using Matlab[®]. Two such images, and corresponding binary edge contours, are presented in Fig. 1, where we can see the initially cylindrical liquid column and the breaking; the time stamp marks the day-of-the-year (1993) and time (GMT). An air bubble about 1 cm in diameter was involuntarily introduced when injecting the liquid through a central 10 mm hole in the lower disc, the one that is moving down to stretch the liquid column. The liquid column is held connected by capillary forces, which restore the shape if the configuration is stable (i.e., if perturbations increase the interface area). A carefully prepared transparent grid with $10 \times 10 \text{ mm}^2$

squares, was glued to the rear window of the experiment cell (80 mm behind the axis of the column), with a white diffuser for background illumination by means of a matrix of 9×8 LEDs. The liquid is a silicone oil 10 times more viscous than water (water was to be avoided at the time), with properties at 20°C : $\rho = 920 \pm 1 \text{ kg/m}^3$, $\sigma = 0.019 \pm 0.0005 \text{ N/m}$, and $\nu = (10 \pm 0.5) \times 10^{-6} \text{ m}^2/\text{s}$ (10 cSt). Ambient cabin air is all around.

A small tilting of the column axis (1.03° clockwise) may be appreciated in the raw images in Fig. 1, which gives an apparent counter-clock tilting of the processed frames being straightened to perform a line-by-line horizontal liquid diameter finding, from the 576 pixel by 720 pixel digitized image. The explanation of such gross misalignment in a high-precision apparatus is due to a late request from the experimenters when they realised that the video camera was oriented to cover the field of view with optimal resolution instead of thinking on post-flight analysis.

The liquid column was attached to two equal discs of radius $R_0 = 15.00 \pm 0.01 \text{ mm}$, made of aluminium black-anodized, having a 30° dove-tail cut back (to enhance cantotaxis) to a 27 mm in diameter stem protruding 12 mm from a base plate to enhance visualisation. Notice the small axial dimension of the cutback: $((30 - 27)/2)\tan 30^\circ = 0.87 \text{ mm}$. A linear potentiometer was used to measure every second disc separation, L , which was $85.0 \pm 0.05 \text{ mm}$ at the beginning, and $93.9 \pm 0.05 \text{ mm}$ at

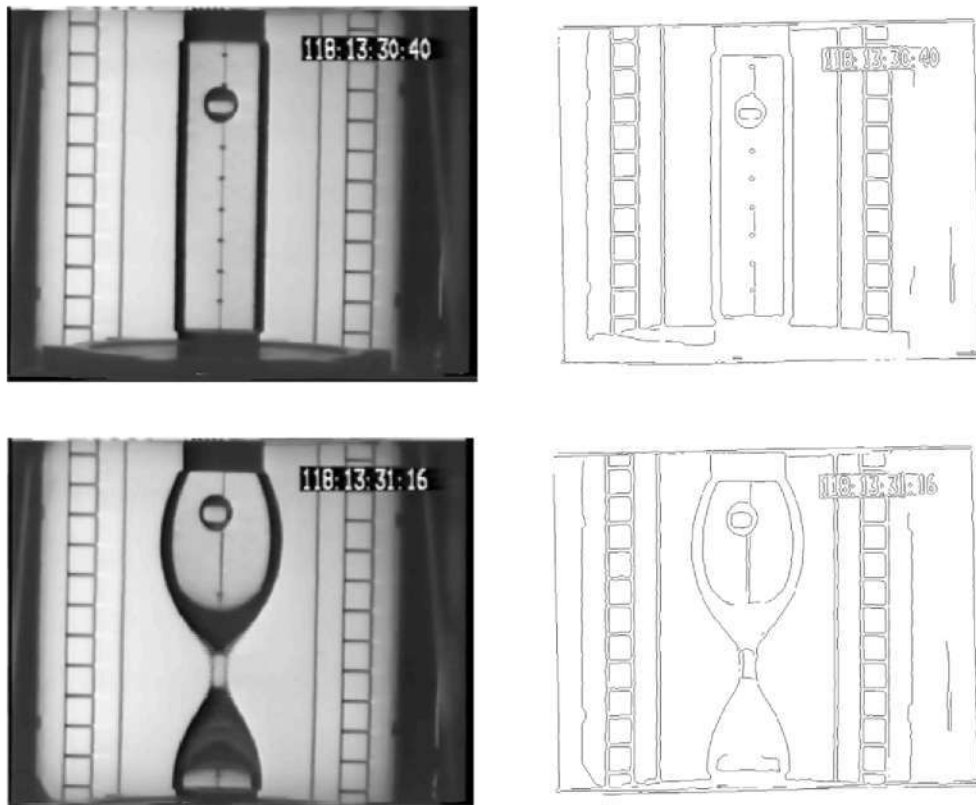


Fig. 1. Video frames of the liquid column at the start of the stretching, and at the breaking point, and their corresponding edges automatically extracted (with the small tilting corrected).

the end of the stretching in this run 2. Liquid volume was measured by another potentiometer in the reservoir piston, indicating a constant value of $59.8 \pm 0.1 \text{ cm}^3$ against the nominal setting of 60 cm^3 , although the large uncertainty due to the entrained bubble is not accounted for. The experimenters had stated in the operational procedures to perform a disc separation from $L = 85 \text{ mm}$ to 95 mm (intended to exceed the limit of stability) without modifying the former separation-rate setting of $dL/dt = 0.72 \text{ mm/s}$ used to fill the liquid at $0.50 \text{ cm}^3/\text{s}$ to have cylindrical column build-up. After flight, we realised that, instead of a constant separation rate, the potentiometer record fitted to $dL/dt = ct$, i.e. a parabolic law with $c = 0.021 \text{ mm/s}^2$, growing from 0 to 0.72 mm/s and lasting 27 s , instead of a linear law with a duration of $(93.9 - 85)/0.72 = 12.6 \text{ s}$. When we asked the manufacturers about that, they said “a slow ramp is implemented and controlled by software in the starting mechanism to avoid jolts and overshootings”. We were fortunate to have a smooth ramp to avoid kicks, which require decay times of 45 s to dump (half way).

The background grid consists of an axial line with tick marks every 10 mm (which can be seen through the transparent liquid column when the dioptrics do not bend light rays too much), a clean line 35 mm off-axis at each side (to be used as calibration for column radii), and a band of 10 mm squares-ladder further away at each side of the axis, all drawn with 1 mm thick black lines (post flight check of raster dimensions showed negligible horizontal distortion, but a dilatation of 0.5 mm and 0.8 mm between extremes corners (130 mm apart along the vertical direction in Fig. 1).

The aim of this experiment was to carry out a controlled breaking of the liquid column by disc separation. The stretching started at point A in the L - V diagram of Fig. 2. The cylindrical column at point A ($L = 85 \text{ mm}$, $V = 60 \text{ cm}^3$) had been established well before (at GMT

118/13:20:55) and left idle (i.e. without applying stimuli) to sense the effect of ambient disturbances, while the investigator on ground gave the operator in space the last instructions (and asked for some optical adjustments: zooming, panning, tilting, etc.); no liquid motion was apparent during these 7 min (the bubble drifted less than 1 cm), and the residual acceleration appears to be below $5 \mu\text{g}$ judging from the minute amphora-type deformation of the cylindrical column, well in accordance with the microgravity accelerometer’s reading near the AFPM that showed $g_{Y,\text{max}} < -0.5 \mu\text{g}$ in that period (along the axial direction). Then, the column length L was increased (separating the lower disc in Fig. 1) while keeping the volume V constant, thus going through the path A to B in Fig. 2, and beyond, to guaranty that the column would break, a recoverable event according to previous practice in Spacelab D-1 in 1985, but which proved unrecoverable in all of our Spacelab D-2 experiments.

2. Experiment results

Let introduce the non-dimensional variables $v \equiv V/(\pi R^2 L) - 1$ and $\lambda \equiv L/(2\pi R) - 1 = A/\pi - 1$ (with $A \equiv L/(2R)$ being the slenderness), which measure the volume departure from a cylindrical column and the slenderness approach to the cylindrical limit $L_{\text{max,cyl}} = 2\pi R$ (Plateau-Rayleigh stability limit). The A-to-B path in Fig. 2 corresponds to the relationship $(1+v)(1+\lambda) = V/(2\pi^2 R^3) = 59.8/(2 \times \pi^2 \times 1.5^3) = 0.898$, with $v_A = -0.0047$ (i.e. a very small departure from cylindrical shape $v = 0$) and $\lambda_A = -0.0981$ (nominal, close to critical slenderness). The stability limit close to the cylindrical shape (the ascending curve passing by B in Fig. 2) can be linearly approximated by $v = 2\lambda$, or better by $v_{\text{min}} = 2\lambda + (5/2)\lambda^2$ or $\lambda_{\text{max}} = v/2 - v^2/3$. Table 1 gives the parameter values at the key points in the experiment based on potentiometer records of $L(t)$ and $V(t)$, accurate to 1 s . The instant of bridge disruption is accurate to a single video-frame ($1/25 \text{ s}$), and that instant has been taken as time reference ($t = 0$) in what follows. The stability margin, s , is computed by evaluating $s(t) = v(t)/2 - \lambda(t)$, with $s = 0$ marking the stability limit.

From now on, the experiment analysis is based just on the video images, using the scale factor from the discs diameter: $2R = 30 \text{ mm}$ to 138 pixels at the object plane. Notice that some image distortions due to complicated optical path (with three mirrors, and eccentric camera pivoting) are unavoidable. We have not made use of some few hard copies available from the 36-exposures 35-mm photo film shot within the AFPM during the whole Spacelab flight.

At every image, once straighten, automated edge extraction is performed using the Canny algorithm in Matlab (it finds edges by looking for local maxima of the gradient of the grey-level matrix, using the derivative of a Gaussian filter). Some manual inspection of the extracted edges around the solid discs allow to fix the disc diameter as $138 \pm 1 \text{ pixels}$, the upper disc (upper end of the liquid column in

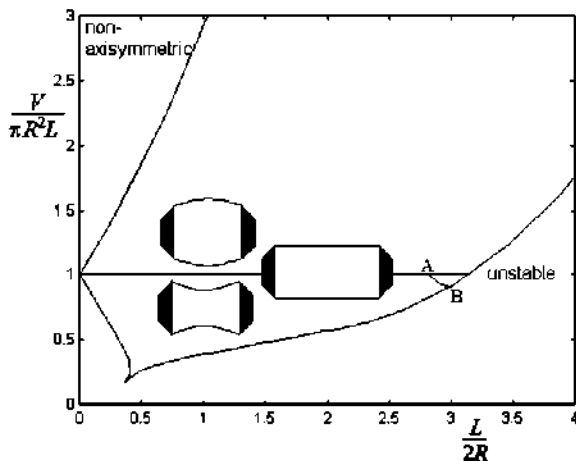


Fig. 2. Stability diagram for unloaded liquid bridges of volume V between equal discs of radii R a distance L apart [Da Riva and Martínez, 1979], with the experiment sequence from A to B.

Table 1

Experimental values corresponding to the sequence analysed (from the end of optical adjustment, to the breaking point, $t = 0$).

Event	GMT [s]	t [s]	L [mm]	$A \equiv (2R)$	$\lambda = A/\pi - 1$	$v \equiv V/(\pi R^2 L) - 1$	$s \equiv v/2 - \lambda$
Liquid column idle	118:13:28:23	-173	85.0	2.83	-0.098	-0.005	0.096
Start of stretching	118:13:30:39	-36.5	85.0	2.83	-0.098	-0.005	0.096
Stability limit	118:13:31:02	-14.5	90.9	3.03	-0.034	-0.070	0
End of stretching	118:13:31:07	-9.5	93.9	3.13	-0.004	-0.099	-0.046
Breaking (last bridge)	118:13:31:16	0	93.9	3.13	-0.004	-0.099	-0.046

Fig. 1) at 66 ± 2 pixels from the top, and the lower disc, initially at 505 ± 2 pixels from the top, before stretching the liquid column by lower disc separation to pixel 548 ± 2 (raw images have 576 pixel vertically, but have 589 pixels after automated straighten them 1.03°). These rough sizes and positioning become much more accurate when taking statistical averages from the several thousand images scanned (25 fps). Notice that a 85 mm liquid column seems to measure more than eight-and-a-half background squares of 10 mm, because there is a 110% column magnification due to conical viewing; the grid is 80 mm behind the column axis, and the camera lens is 800 mm in front.

The motion of the discs (the lower disc in our case, since the upper disc remains fixed in this experiment, but was moving up and down in Staco run 1), is automatically detected by following the edge of the base plate attached to the disc, since the latter cannot easily be followed because of the liquid dioptrics and the smallness of their dove-tail.

At every cross-section in the liquid zone, the semi-difference of the edge position gives the radius, and the semi-sum the central position of the liquid slice (small lateral motion of the liquid column can also be appreciated). These single values have an uncertainty of one pixel, but we get a much better accuracy by fitting the whole liquid outline at every image with a Fourier series expansion; in this experiment, retaining just the first term in sine and in cosine is good enough to fit any liquid shape except those close to breaking (where two or three additional terms are needed). The vertical distribution of radii in the liquid column is to be approximated in every image, in non-dimensional variables centred at the column mid-plane, by (Martínez et al., 2005):

$$r(z, t) = 1 + \frac{v(t)}{2} \left(1 + \cos \frac{\pi z}{\Lambda(t)} \right) + a(t) \sin \frac{\pi z}{\Lambda(t)} \quad (1)$$

with $-A < z < A$, and where the explicit dependence of each variable has been stated: $\Lambda(t)$ is the time-varying slenderness in this stretching experiment, $a(t)$ is the amplitude of the amphora-type deformation of the column (due to dynamic effects in this experiment, since the residual acceleration was negligible), and $v(t) = V/(\pi R^2 L(t)) - 1$ (liquid volume, V , is preserved).

The raw values (in pixels with origin in the top-left corner) obtained when fitting the liquid column radii extracted from each image to a sine plus a cosine with the period of the whole span, $z_{i,\text{top}} < z_i < z_{i,\text{bottom}}$; i.e.:

$$r_i(z_i) = r_{i,\text{mean}} + b(t) \cos \frac{2\pi z_i}{z_{i,\text{bottom}} - z_{i,\text{top}}} + a(t) \times \sin \frac{2\pi z_i}{z_{i,\text{bottom}} - z_{i,\text{top}}} \quad (2)$$

are presented in Fig. 3 for the last 50 s of the breaking process. Besides these first terms in sine and cosine, $a(t)$ and $b(t)$, higher terms are also plotted, showing up only in the last 3 s before breaking, when column deformation is too large for Eq. (1) to be applicable.

The sine amplitude (i.e. that of the amphora-type liquid shape), $a(t)$, oscillates in time with an amplitude peak-to-peak of 1.4 pixels (0.3 mm) and a period around 14 s when the column is idle, corresponding to the first axial eigenfrequency of this liquid configuration, as predicted by theory (Meseguer, 1983; Montanero, 2003; Ferrera et al., 2006), and then diverges after the stability limit is crossed at $t = -14.5$ s (marked with a "*" in Fig. 3), with an initial time-to-double-amplitude of $T_2 = 2.7 \pm 0.5$ s, found by fitting that $a(t)$ curve to $a(t) = a_0 \exp((t/T_2) \ln 2)$.

The amplitude of the spindle-like liquid shape, $b(t)$ in Eq. (2), starts with a steady value of -0.2 pixels (undetectable to the necked eye), and grows to some 4 pixels during the stretching of the column, in accordance with the spindle shape produced in an initially cylindrical liquid column when the end discs are separated while maintaining the

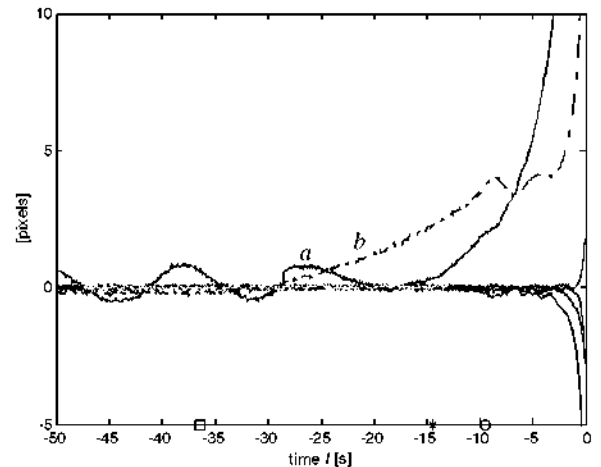


Fig. 3. Sine amplitude a , cosine amplitude b , and higher order Fourier terms (only visible in the last 4 s). The end point ($t = 0$) corresponds to column disruption (the video frame shown at the bottom in Fig. 1). Disc separation starts at $t = -36.5$ s (\square -mark) and ends at $t = -9.5$ s (\circ -mark). The column becomes unstable at $t = -14.5$ s ($*$ -mark).

liquid volume constant (evolution A to B in Fig. 2). The small dip in $b(t)$ after the stretching stops (at $t = -8$ s in Fig. 3), seems to be due to the dynamic bouncing in the liquid shape by the sudden disc-stop.

The relative uncertainty in the obtained radial shape parameters $a(t)$ and $b(t)$ is very low, well below a tenth of a pixel (of the order of $10\ \mu\text{m}$ in real size, about 0.07% of disc radius), since, by taking more than 400 radii in every image to compute the sine or cosine amplitude, the uncertainty reduces more than $\sqrt{400} = 20$ times. However, the relative uncertainty in axial distances is larger: some 2.5% (instead of 0.07%) for the computed length of the column from the images, as shown in Fig. 4. Non-square pixel size cannot explain that discrepancy; in fact, the background grid (Fig. 1) has been used to find the vertical/horizontal pixel ratio $\text{PR} = 1.095 \pm 0.005$ and already corrected. To make the problem simpler, the slenderness of the stretched column $A_1 = 93.9/30$, divided by the slenderness of the unstretched column $A_0 = 85/30$, measured from many images in raw units yield a value of 1.12 ± 0.01 instead of $A_1/A_0 = 93.9/85 = 1.105$, ruling out a simple scaling amendment.

The measured liquid volume performed by integration of the column slices has a relative discrepancy of $1.9\ \text{cm}^3$ over the $59.8\ \text{cm}^3$ indicated by the potentiometer in the liquid reservoir piston, but this discrepancy (3.2%) is to be expected from the bubble problem found in the liquid injection. However, the fact that the volume is bigger than the cylindrical one is consistent with the constant value $b = -0.2$ pixels mentioned above, which implies that there was some $v = -b/r_0 = 0.2/69 = 0.003$ excess nondimensional volume (i.e. $0.17\ \text{cm}^3$). The last plot in Fig. 4 corresponds to the stability margin $s = -\lambda + v/2$, which, with the potentiometer data for $\lambda(t)$ and the stretching law $(1+v)(1+\lambda) = V/(2\pi^2 R^3) = 0.898$, define the adopted stability limit (solving $-\lambda + v/2 = 0$), $t = -14.5$ s (marked with '*'); notice that, from image data with all uncertainties

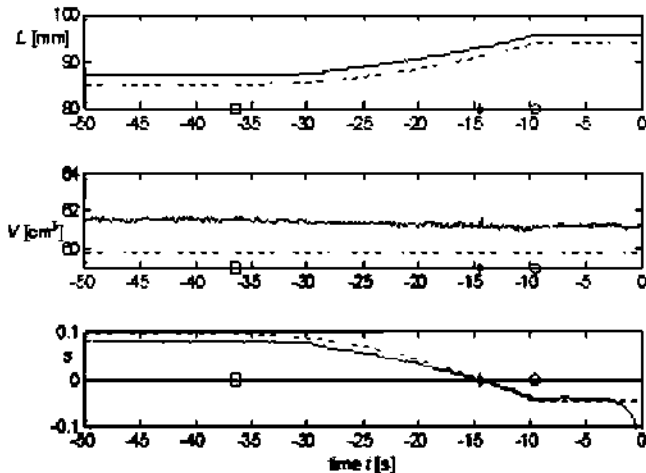


Fig. 4. Comparison of image-based values (solid lines) with potentiometer readings (dash lines) for column length, L , column volume, V , and nondimensional stability margin, $s \equiv v/2 - \lambda$. Time marks as in Fig. 3.

mentioned and some possible dynamic effect, the stability crossing is at -15.0 s instead of -14.5 s.

Coming back to the radial evolution on breaking, Fig. 5 presents the necking details: minimum radius, its axial position, and the corresponding partial volume fraction up to this point. The extracted shape corresponding to the last liquid-bridge before breaking (pictured in Fig. 1), is also included. The formation of a satellite drop from the long neck, after breakage, is clearly seen in the video record (Martínez, 2010).

3. Dynamic simulation

Consider a long axisymmetric liquid column, close to its axial stability limit. If only the first natural mode is excited, the dynamic shape, in nondimensional units, can be approximated as:

$$r(z, t) = r_{eq}(z) + a(t) \sin \frac{\pi z}{\Lambda} \quad (3)$$

where $r_{eq}(z)$ is the equilibrium shape (i.e. for $a = 0$, which can be computed with the Young–Laplace capillarity equation; in our case, a symmetric spindle shape at any point in between A and B in Fig. 2). The dynamic evolution of the liquid shape, measured by the sine amplitude $a(t) \neq 0$, is governed by the Duffin's type equation first deduced by Rivas and Meseguer, 1984 (see Martínez et al., 2005, but mind a sign mistype in that equation there, not in the computed results):

$$m \frac{d^2 a(t)}{dt^2} + mC \frac{da(t)}{dt} + \left(\frac{v}{2} - \lambda\right) a(t) - \frac{3}{4} a(t)^3 = 0 \quad (4)$$

where $m = 3.17$ is a non-dimensional inertia-term coefficient (3.13 if deduced with Cosserat model), and $C = Oh^{1/2} = v(\rho/(\sigma R))^{1/2} = 0.0175$ is the square root of the Ohnesorge number accounting for viscous dissipation

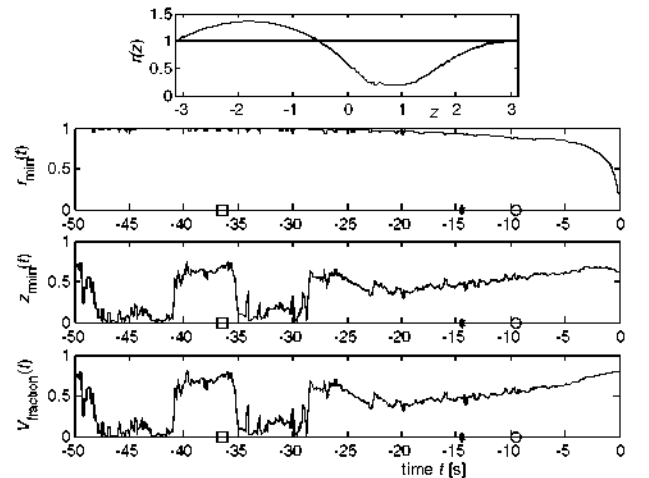


Fig. 5. Above, last shape analysed in the automated sequence (the video frame in Fig. 1). Below, evolution with time of minimum radius, r_{\min} (relative to disc radius), its axial position, z_{\min} (relative to column length, from top), and volume fraction of liquid up to the position of minimum radius, V_{fraction} .

(with $\nu = 10 \times 10^{-6} \text{ m}^2/\text{s}$, $\rho = 920 \text{ kg/m}^3$, $\sigma = 0.020 \text{ N/m}$). Lengths are made nondimensional with $R = 0.015 \text{ m}$, and time is made non-dimensional with $(\rho R^3/\sigma)^{1/2} = 0.394 \text{ s}$.

Let first consider nonlinear effects from Eq. (4) for the stability margin that we have been used linearised to $\nu/2 - \lambda > 0$ up to now. Deleting the dynamic terms in Eq. (4), and dividing by a , one gets the static solutions:

$$\left(\frac{\nu}{2} - \lambda\right) - \frac{3}{4}a^2 = 0 \quad (5)$$

with $a = 0$ being the stable equilibrium amplitude, and $a = \pm 2\sqrt{(\nu/2 - \lambda)/3}$ the unstable equilibrium amplitude. All dynamic solutions with $0 < |a| < |a|_{\max} = 2\sqrt{(\nu/2 - \lambda)/3}$ correspond to stable amphora-type deformation in a potential well with the bottom at $a = 0$. We have plotted in Fig. 6 the value of a_{\max} in our experiment with the stretching law $(1 + \nu)(1 + \lambda) = V/(2\pi^2 R^3) = 0.898$, and for the all-cylindrical sequence ($\nu = 0$), $a_{\max, \text{cyl}} = 2\sqrt{-\lambda/3}$, but using dimensional value scaled with the 15 mm disc radius, including the actual amplitude $a(t)$ found from the images at its corresponding length, to see if the crossing of the stability limit was at a distinct slenderness than assumed ($a = 0$ was used to compute the stability limit from $\nu/2 - \lambda = 0$), realising that the effect of the running $a \neq 0$ is indeed irrelevant in this experiment.

You may see in Fig. 6 that, before stretching ($L = 85 \text{ mm}$), there are amplitude oscillations (with 0.3 mm amplitude); then the amplitude $a(t)$ waxes a little during the stretching from 85 mm to 93.9 mm, and finally the amplitude grows monotonically at the final setting of $L = 93.9 \text{ mm}$, until breaking.

The linear in viscid dynamics, i.e. neglecting the dissipation and the nonlinear terms in (4), yield the period of the harmonic oscillations in the stable case, T_0 , and the time-to-double amplitude, T_2 , in the unstable case, namely:

$$m\ddot{a} + \left(\frac{\nu}{2} - \lambda\right)a = 0 \begin{cases} \text{if } (\frac{\nu}{2} - \lambda) > 0, & T_0 = 2\pi\sqrt{\frac{m}{-\lambda + \nu/2}} \\ \text{if } (\frac{\nu}{2} - \lambda) < 0, & T_2 = \ln 2\sqrt{\frac{m}{\lambda - \nu/2}} \end{cases} \quad (6)$$

which have been plotted in Fig. 7 in dimensional units (times were scaled with $(\rho R^3/\sigma)^{1/2} = 0.394 \text{ s}$), for our stretching experiment, where ν is related to λ by $(1 + \nu)(1 + \lambda) = 0.898$.

The predicted oscillation period in the unstretched column is $T_0 = 14.2 \text{ s}$ (at $L = 85 \text{ mm}$ in Fig. 7), in perfect agreement with the experimental results ($a(t)$ oscillations in Fig. 3). Although not reported here, the first lateral eigenfrequency of the idle initial column with $L = 85 \text{ mm}$ has a small amplitude (6 pixels, 1.3 mm, peak-to-peak) and a period of $4.5 \pm 0.2 \text{ s}$, as already reported in the former paper by Martínez et al., 1995.

However, the predicted time-to-double-amplitude period in the stretched column given by Eq. (6) is $T_2 = 2.27 \text{ s}$ (at $L = 93.9 \text{ mm}$ in Fig. 7), whereas the experimental results (diverging $a(t)$ in Fig. 3) fits best to $T_2 = 3.0 \pm 0.1 \text{ s}$ in the initial stage, as depicted in Fig. 8 (dash line). A possible explanation might be that the final length is reached after passing in 5 s (from -14.5 to -9.5) through stages with larger time-to-double-amplitude periods (e.g. region around $L = 92 \text{ mm}$ in Fig. 7), but we have found a perfect explanation in the non-linear term in Eq. (4); if we integrate the complete differential Eq. (4) (the dissipation term is irrelevant for the short times envisaged and can be skipped), to find $a(t)$ from the end-of-stretching state, i.e. from $t_0 = -9.5 \text{ s}$ up to $t = 0$ in Fig. 3, with the initial conditions at that time, $a(t) = 0.026$ (0.4 mm, 1.8 pixels) and $\dot{a}(t) = 0.0016$ (0.06 mm/s, 0.3 pixels/s), we get an amplitude evolution that perfectly matches the experimental one (the upper one of the two solid lines in Fig. 8; the lower one being the set of experimental points).

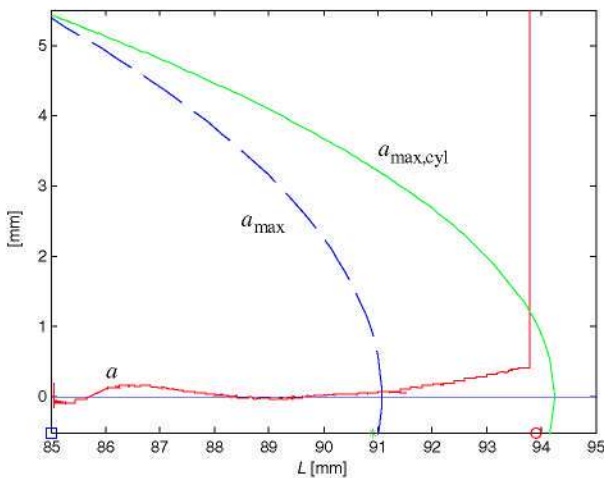


Fig. 6. Evolution of amphora-type dynamic amplitude, a , as a function of corrected column length $L(t)$, with maximum stable amplitude for our constant volume experiment, a_{\max} , and maximum amplitude for a cylindrical stretching, $a_{\max, \text{cyl}}$ (which coincides before stretching at $L = 85 \text{ mm}$, and cancels at the Plateau-Rayleigh limit, $L = 2\pi R = 94.2 \text{ mm}$).

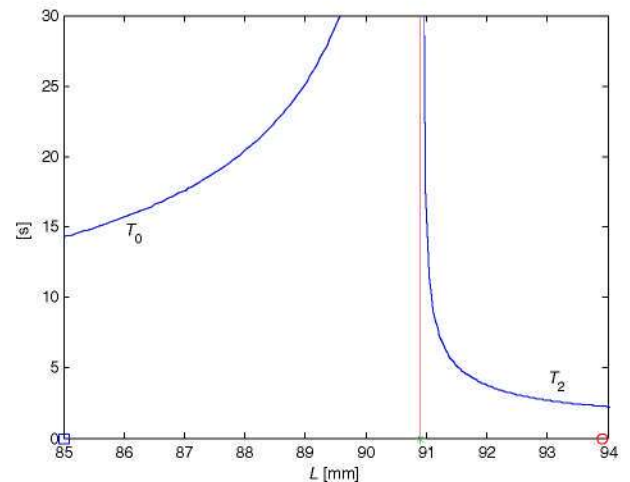


Fig. 7. Oscillation period for stable columns, T_0 , and time-to-double-amplitude, T_2 , in the unstable case, for liquid columns during slow stretching at constant volume, as a function of disc separation L .

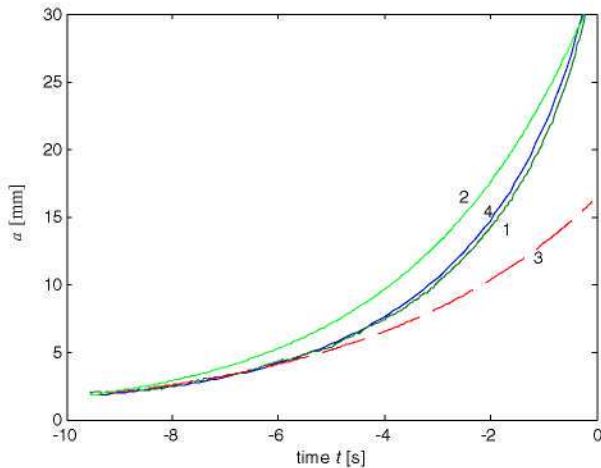


Fig. 8. Comparison of the diverging amplitude of the amphora-type deformation (last part of Fig. 3): (1) experimental points; (2) linear dynamics simulation, $a(t) = a_0 \exp((t/T_2) \ln 2)$, using the theoretical result $T_2 = 2.27$ s; (3) linear dynamics simulation with best initial fit ($T_2 = 3$ s); (4) non-linear simulation with Eq. (4).

4. Conclusions

We have made here a detailed analysis of a unique experiment performed in 1993 aboard Spacelab (D-2 mission), making use of the new image-analysis tools not available at the time when the first analysis of this experiment was published (Martínez et al., 1995). The former analysis concluded that the stable oscillations, both axial and lateral, were quantitatively as predicted by linear theory, but the unstable dynamics was not analysed.

Different video sources (recorded aboard, transmitted and recorded on ground) have different time shift and frame size. Besides, different video digitization procedures yield different pixel resolutions. In the former analysis, transversal lines were scanned at 512 pixels, and now we use 720 pixels. But the major difference is on longitudinal lines, that where at the time very difficult to handle; in fact, the moving bottom disc went out of sight at 92 mm, before the 93.9 mm stop, in the old digitization. Lateral oscillations of the centre line and radial evolution were shown at three initially equi-spaced column sections (but the same video-lines were scanned during the stretching sequence, not accounting for the length increase). With the present analysis all these handicaps are overcome.

The perfect matching of the dynamic behaviour shown in Fig. 8 for the unstable evolution to the breaking point adds confidence on the accuracy of Eq. (4) to predict the real behaviour of liquid columns, both in the stable and the unstable regions of the parameter space, at least close to the stability limits, and up to the point where higher order eigenfunctions had to be added to Eq. (3).

As already said, a possible explanation to the fact that the liquid column appears more slender in the images than

in reality (after thorough calibration with the background reference grid), may be that images of the liquid column give always a smaller value for radii due to reflection of the grazing rays, and the parallax effect.

Other minor inconsistencies between the results of the image analysis and what should be expected might be attributed to small mechanical disturbances introduced by the operator or nearby equipment, and not detected on the microgravity measurement assembly (MMA), as the small slips in the twelve near-perfect harmonic oscillations of the liquid column during the 150 s of inactivity preceding the stretching operation. More difficult to explain is why the column maintains the same oscillation amplitude, without decaying, for such a long period, knowing that the natural dumping time, i.e. the period where the amplitude reduces to a half, is some 35 s (Martínez et al., 2005).

Automated image analysis has progressed a lot, but some intrinsic problems of the experiment design cannot be coped with; particularly, details of the disc edges cannot be reconstructed from the old videotapes. Of course, digital imaging nowadays would solve many of the old video problems, but good lessons learnt from past experience will always offer invaluable guidance.

Appendix A. Supplementary data

Supplementary data associated with this article can be found, in the online version, at doi:10.1016/j.asr.2011.03.012.

References

- Da Riva, I., Martínez, I. Floating Zone Stability. ESA SP-142, pp. 67–73, 1979.
- Ferrera, C., Cabezas, M.G., Montanero, J.M. An experimental analysis of the linear vibration of axisymmetric liquid bridges. *Phys. Fluids* 18, 082105–082120, 2006.
- Martínez, I., Perales, J.M., Meseguer, J. Stability of long liquid columns (SL-D2- FPM-STACO), in: Sahn, P.R., Keller, M.H., Schiewe, B., (Eds.), *Scientific Results of the German Spacelab Mission D-2*, WPF, pp. 220–231, 1995.
- Martínez, I., Perales, J.M., Meseguer, J. Non-linear response of a liquid bridge to a sinusoidal acceleration under microgravity. *Exp. Fluids* 37, 775–781, 2004.
- Martínez, I., Meseguer, J., Perales, J.M. Wobbling of a liquid column between unequal discs. *Adv. Space Res.* 36, 26–35, 2005.
- Martínez, I. http://webserver.dmt.upm.es/~isidoro/lc1/SL/ST2_118_13_30_41stretch_xvid.avi, 2010.
- Meseguer, J. The breaking of axisymmetric slender liquid bridges. *J. Fluid Mech.* 130, 123–151, 1983.
- Montanero, J.M. Linear dynamics of axisymmetric liquid bridges. *Eur. J. Mech. B/Fluids* 22, 167–178, 2003.
- Rivas, D., Meseguer, J. One-dimensional self-similar solution of the dynamics of axisymmetric slender liquid bridges. *J. Fluid Mech.* 138, 417–439, 1984.
- Zhang, X., Padgett, R.S., Basaran, O.A. Nonlinear deformation and breakage of stretching liquid bridges. *J. Fluid Mech.* 329, 207–245, 1996.